Konrad KANIA[1,2], Michał MAJ[1,2], Tomasz RYMARCZYK[1,2], Przemysław ADAMKIEWICZ[1,2], Michał GOŁĄBEK[1]

Research & Development Centre Netrix S.A.(1), University of Economics and Innovation (2)

doi:10.15199/48.2020.01.41

Image reconstruction in ultrasound transmission tomography using the Fermat's Principle

Abstract. *The article presents image reconstruction in ultrasonic transmission tomography using the Fermat principle. The application consists of an ultrasound tomograph built by the authors and an algorithm implemented to solve the problem of image reconstruction. The solution enables the analysis of processes taking place in the facility without interference. The obtained tomographic imaging can be a picture of the geometry of the examined area. This allows location in the analysed area. The work developed an algorithm based on the Fermat principle as a technique of low computational complexity for real-time image reconstruction using an ultrasound tomograph..*

Streszczenie. *W artykule przedstawiono rekonstrukcja obrazu w ultradźwiękowej tomografii transmisyjnej z wykorzystaniem zasady Fermata. Aplikacja składa się z tomografu ultradźwiękowego zbudowanego przez autorów oraz zaimplementowane algorytmu do rozwiązywania zagadnienia rekonstrukcji obrazu. Rozwiązanie umożliwia analizę procesów zachodzących w obiekcie bez ingerencji. Uzyskane obrazowanie tomograficzne może być obrazem geometrii badanego obszaru. Pozwala to na lokalizację w analizowanym obszarze. W pracy opracowano algorytm oparty na zasadzie Fermata jako technice o niskiej złożoności obliczeniowej do rekonstrukcji obrazu w czasie rzeczywistym za pomocą tomografu ultradźwiękowego.. (**Rekonstrukcja obrazu w ultradźwiękowej tomografii transmisyjnej z wykorzystaniem zasady Fermata)*.

Keywords: Fermat's principle, ultrasound transmission tomography, image reconstruction.
Słowa kluczowe: zasada Fermata, ultradźwiękowa tomografia transmisyjna, rekonstrukcja obrazu.

Introduction

The construction of a physical model of an ultrasonic tomograph is highly problematic due to the complexity of the acoustic phenomena necessary for modeling in the case of a heterogeneous environment of propagation of acoustic waves in small limited spaces [1]. The radial propagation model commonly used in transmission tomography turns out to be sufficient for effective detection of disturbances in the interior of objects and is used in commercial solutions, for example for non-invasive examination of the state of trees. The lack of the correct physical model does not allow us to fully understand phenomena occurring during imaging with the help of acoustic waves. Problems such as [2-14] are used to solve optimization problems. In tomography, methods [15-25] are used to solve the inverse problem. This work is a collection of numerical experiments that use the Fermat principle, originally used in optics, to better understand the process of acoustic wave propagation during tomographic measurements using ultrasound [26-40] to create a more precise solver for problems with ultrasound tomography.

Algorithm

Classical approach to modeling the ultrasonic tomographical system is to approximate the behavior of the system by the model of straight rays of propagation between two ultrasonic sensors. There are many works confirming the effectiveness of such a solutions in the terms of reliable ability of imaging positions of inclusions along the domain of tomographical system. The effectiveness of that types of models can be also confirmed by practical analysis of a measurement data from tomographical device. As the example Figure 2 shows the sensitivity visualization of the tomographical system. Presented visualization is made for one pair of sensor and is created on the basis of real measurement data with one air inclusion with water background. One can see that higher sensitivity is concentrated approximately along the line between the sensors. Despite that facts there is still no good physical model for the UST therefore any attempt of getting more insight in the field is desirable.

Fermat's principle describe how disorder is spreading in inhomogeneous media. Classically, the Fermat principle for a light ray can be expressed as: if a light ray is moving from point A to B, in a heterogeneous optical medium, there will be a path that will minimize the transition time between these points. The current version of this principle says that the disorder, in a heterogeneous medium, propagates through *stationary* curves. The stationary condition means that the curve does not have to minimize the transition time, it is enough that it meets the necessary condition of its existence from the point of view of the variational calculus.

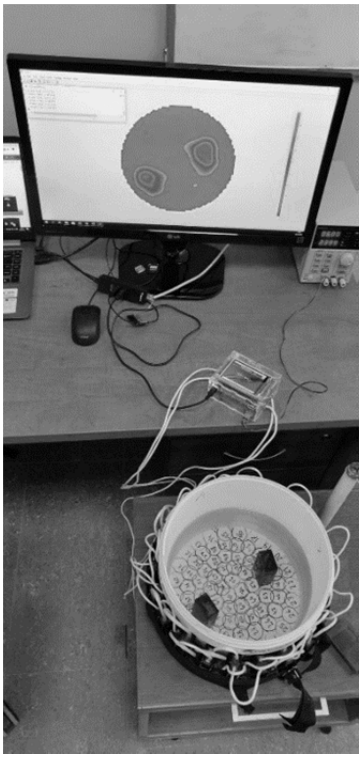

Fig. 1. Measurement system.

Due to the use in tomography, we consider a two-dimensional space. Let us assume that the disturbance in a heterogeneous medium propagates from the point $A(x_0, y_0)$ to point $B(x_1, y_1)$ along the curve described in the Cartesian coordinate system with the functional dependence

(1) $y = y(x)$.

The inhomogeneity of the medium is determined by the function assigning to each point of the space the value of the propagation speed of the disorder at a given point: $v = v(x, y)$.

The function of the transition time of the disturbance from point A to point B has the form

(2) $T[y] = \int_{x_0}^{x_1} F(x, y, y')dx = \int_{x_0}^{x_1} f(x, y)\sqrt{1 + (y')^2}\, dx,$

where $f(x, y) = \frac{1}{v(x,y)}$

Let's consider the Euler's differential equation for this type of functionals

$$\frac{\partial F}{\partial y} - \frac{d}{dx}\left(\frac{\partial F}{\partial y'}\right) = f_y(x, y)\sqrt{1 + y'^2} - \frac{d}{dx}\left[f(x, y)\frac{y'}{\sqrt{1 + y'^2}}\right]$$

$$= f_y(x, y)\sqrt{1 + y'^2} - f_x\frac{y'}{\sqrt{1 + y'^2}} - f_y\frac{y'^2}{\sqrt{1 + y'^2}} - f\frac{y''}{\left(\sqrt{1 + y'^2}\right)^3}$$

$$= \frac{1}{\sqrt{1 + y'^2}}\left[f_y - f_x y' - f\frac{y''}{1 + y'^2}\right] = 0$$

Hence the condition from Euler's equation has a form

(3) $f_y - f_x y' - f\frac{y''}{1+(y')^2} = 0.$

The stationary condition for the transition curve y = y (x) means, therefore, that the curve is a solution to equation (3).

Euler equation solution

By determining the second derivative from the Euler equation quoted above, we obtain the equation

(4) $y'' = (1 + (y')^2)\left(\frac{f_y}{f} - \frac{f_x}{f}y'\right).$

Using substitutions $t = x,\ y_1 = y,\ y_2 = y'$, this equation can be transform to the system of first order equations

(5) $$\begin{cases} y_1' = y_2 \\ y_2' = (1 + y_2^2)\left(\frac{f_y}{f} - \frac{f_x}{f}y_2\right) \end{cases}$$

In numerical experiments, it was assumed that in the working space of a tomograph (a circle with a radius $R = 5$) there was a single circular inclusions with a radius $r_w = 1$. To be able to solve the derived system of equations, the distribution of velocities of sound propagation in the working area was modeled with rotating surfaces with equations

(6) $v_1(r) = (b - w)\left(\frac{r^{2n}}{r^{2n}+1}\right) + w, \quad if\ b \geq w$

(7) $v_2(r) = (w - b)\left(1 - \frac{r^{2n}}{r^{2n}+1}\right) + b,\ if\ b < w$

Because these functions boil down to one equation

(8) $f(x, y) = \frac{1}{v(x,y)} = \frac{C(x,y)}{M(x,y)} = \frac{(x^2+y^2)^n+1}{b(x^2+y^2)^n+w}$

The idea of that model for distribution comes from the fact that functional series $a_n(x) = \frac{x^n}{x^n+\rho^n},\quad x \in [0, +\infty]$ for $n \to \infty$ tends to the discontinuous unit jump at $x = \rho$, hence by using big enough value of n one can approximate a discontinuous boundary of the inclusions.

In the equations (6-8) b is a speed associated with the background medium and w is a speed of sound for the included object.

Using the defined speed distribution, we get that

(9) $C_x = 2xn(x^2 + y^2)^{n-1},$

(10) $C_y = 2yn(x^2 + y^2)^{n-1}$

(11) $M_x = bC_x, M_y = bC_y.$

Hence

$$\frac{f_x}{f} = \left(\frac{C_x M - C M_x}{MC}\right) = C_x\left(\frac{M - bC}{MC}\right) = C_x\left(\frac{w-b}{MC}\right) \quad (12)$$

$$\frac{f_y}{f} = \left(\frac{C_y M - C M_y}{MC}\right) = C_y\left(\frac{M - bC}{MC}\right) = C_y\left(\frac{w-b}{MC}\right). \quad (13)$$

That mean that

(12) $y'' = 2n(x^2 + y^2)^{n-1}(1 + (y')^2)\left(\frac{w-b}{MC}\right)(y - xy').$

Hence the system of equations (5) takes the form

(13) $$\begin{cases} y_1' = y_2 \\ y_2' = 2n(t^2 + y_1^2)^{n-1}(1 + y_2^2)\left(\frac{w-b}{MC}\right)(y_1 - ty_2) \end{cases}$$

This system can be solved using numerical methods. In the case of this work, the one-step Runge-Kutta method of the fourth order was used. The initial condition imposed on y_1 determines the location of the starting point of the disturbances while the condition for y_2 determines the initial direction of its propagation.

For the purposes of the experiment, a beam of rays coming from one probe located at $(-R, 0)$ was considered. The beam consisted of 151 rays was propagating in the range of $\pm 45°$.

At this point it is worth noting that the reconstructed curves in the general case do not formally form the curves described by functional equation (1), natural way to generalize the problem was usage of parametrical curves with a natural parametrization i.e. with a parameter associated with the partial length of the propagated curve. However, when trying to reformulate the task using the parametric description of the curves, two significant problems were encountered:

Firstly, there is a theorem known from variational calculus:

The sufficient and necessary condition for independency of the value of a functional

(14) $\int_{t_1}^{t_2} \theta(t, x, y, \dot{x}, \dot{y})dt$

from the parametrical description of the curve is that the function doesn't explicitly depends on t and is positively homogeneous due to the $\dot{x}, \dot{y}$.

In our situation the functional meets the assumptions of that theorem therefore its value is independent from the parametric description of the curve. This freedom of parameterization greatly hinders the adoption of specific ranges for the parameter describing the curve, and thus makes it difficult to define the range to be solved by the obtained equation. Secondly, the parametric form of the equation is complicated so much that numerical errors cease to be negligible, and in extreme cases numerical solvers are not able to obtain a stable solution.

To overcome that problems we exploit the features of the stepwise numerical methods of solving the differential equations. The stepwise methods allow, due to their nature, to break the calculations at the moment when the reconstructed curve distorts itself enough to cease to have a functional character in considered coordinate system. Written program to solve this system after detection of such a point, changes the axes of the coordinate system, and from the stopping point reconstructs the curve further but this time in the form of the function x = x (y). If the program encounters the same problem again, it can go back to the description in the form y = y (x). As a result, it is possible to

determine the entire curve, using a non-parametric description, by breaking the curve into disjoint parts that can be described in a functional manner.
Let's notice that for the curve of the form

(15) $$x = x(y),$$

associated functional is

(16) $$T[x(y)] = \int_{y_0}^{y_1} g(x,y)\sqrt{1+(x')^2}\,dy.$$

Notice that in the case of one inclusion centered in the domain

(17) $$g(x,y) = f(y,x) = f(x,y) = \frac{(x^2+y^2)^n+1}{b(x^2+y^2)^n+w},$$

hence the Euler's equation is

(18) $$f_x - f_y x' - f\frac{x''}{1+(x')^2} = 0$$

And

(19) $$x'' = (1+(x')^2)\left(\frac{f_x}{f} - \frac{f_y}{f}x'\right),$$

what means that using analogous substitutions $y = t,\ y_1 = x,\ y_2 = x'$, the systems of DEs are equivalent so there is no need for solving another system after switching the coordinates.

IV. Case of a off-center inclusion

In the case when single inclusion is not centered in a tank the distribution of velocity is changed. If the centrum of the circular inclusion is located in a point (a,b) (in the Oxy plane) the functions in the time-of-fly functionals take the forms

(20) $$f(x,y) = g(x,y) = \frac{1}{v(x,y)} = \frac{C(x,y)}{M(x,y)} = \frac{([x-a]^2+[y-b]^2)^n+1}{b([x-a]^2+[y-b]^2)^n+w}$$

One can check that from properties analogical to (9)-(13) the differential equations of second order are

(21) $$y'' = P(x,y,y')\left(\frac{w-b}{MC}\right)(1+(y')^2)(y-b-(x-a)y')$$

for curves of type (1) and

(22) $$x'' = P(x,y,y')\left(\frac{w-b}{MC}\right)(1+(y')^2)(x-a-(y-b)x')$$

for curves of type (18).
where

(23) $$P(x,y,y') = 2n([x-a]^2+[y-b]^2)^{n-1}$$

That means that, after the substitutions we end up with two non-equivalent systems:
For curves of type (1)

(24) $$\begin{cases} y_1' = y_2 \\ y_2' = (1+y_2^2)\left(\frac{w-b}{MC}\right) Q_1(t,y_1)\,(y_1 - b - (t-a)y_2) \end{cases}$$

where $Q_1(t,y_1) = 2n[(t-a)^2+(y_1-b)^2]^{n-1}$.
For curves of (18)

(25) $$\begin{cases} y_1' = y_2 \\ y_2' = (1+y_2^2)\left(\frac{w-b}{MC}\right) Q_2(t,y_1)\,(y_1 - a - (t-b)y_2) \end{cases}$$

where $Q_2(t,y_1) = 2n[(t-b)^2+(y_1-a)^2]^{n-1}$.

Results

In this part, we present the results of numerical experiments (Fig. 2) for inclusions (w = 350, w = 5500) immersed in water (b = 1600) and inclusion (w = 5500) in the air (b = 350).

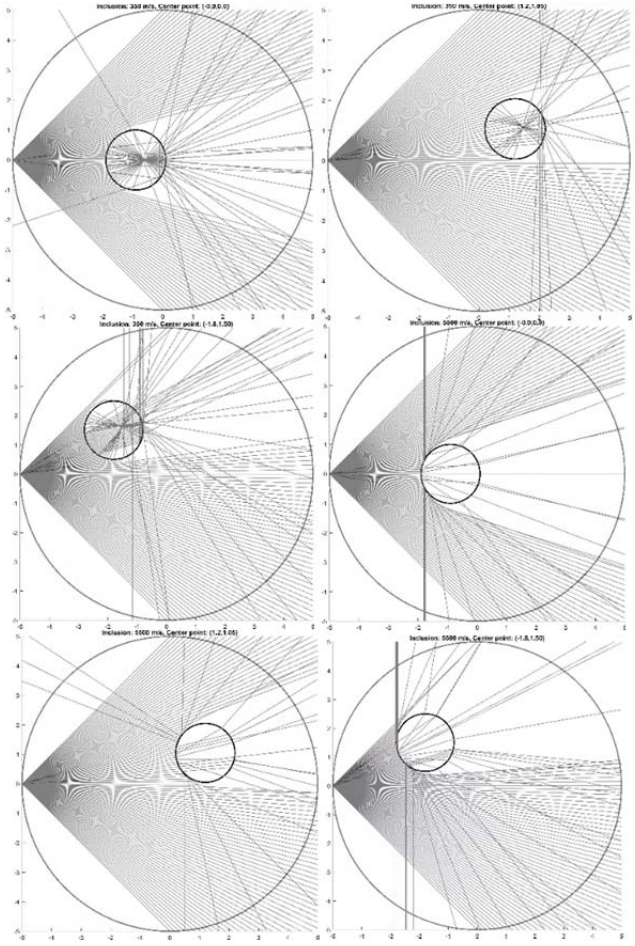

Fig. 2. Ray simulations I for the water background due to the location of the center point of circular inclusion.

Conclusion

In the article image reconstruction using the Fermat principle during tomographic measurements using ultrasound. The system consists of an ultrasound tomograph and an algorithm for solving the inverse problem for image reconstruction. Ultrasound transmission tomography enables the analysis of processes occurring in an object without interfering with it. The obtained tomographic imaging can be a picture of the geometry of the examined area. The presence of inclusions creates a lensing effect. The nature of the deflection depends on the relationship between the background parameter and inclusions. In the case of scattering, the reflection effect of the wave is clearer and less rays penetrate the inclusions. Regardless of the inclusions, the sensor covering effect is noticeable by diluting the beam. The thinning of the beam may translate into a decrease in the density of acoustic energy reaching the sensor, which may be the reason for the increase in the measured transition time - regardless of the material from which the inclusions are made.

***Authors**: Konrad Kania, University of Economics and Innovation, Projektowa 4, Lublin, Poland/ Research & Development Centre Netrix S.A. E-mail: konrad.kania@netrix.com.pl; Michał Maj, University of Economics and Innovation, Projektowa 4, Lublin, Poland/ Research & Development Centre Netrix S.A. E-mail: michal.maj@wsei.lublin.pl; Przemysław Adamkiewicz, Ph.D.., University of Economics and Innovation, Projektowa 4, Lublin, Poland/ Research & Development Centre Netrix S.A. E-mail: p.adamkiewicz@netrix.com.pl; Michał Gołąbek, Research & Development Centre Netrix S.A., E-mail: michal.galabek@netrix.com.pl.*

REFERENCES

[1] Kania K., Rymarczyk T., Maj M., Golabek M., Implementation of fermat's principle for detection of anomalies in ultrasound transmission tomography, 2019 Applications of Electromagnetics in Modern Engineering and Medicine, PTZE 2019, 2019, 67-71

[2] Goetzke-Pala A., Hoła A., Sadowski Ł., A non-destructive method of the evaluation of the moisture in saline brick walls using artificial neural networks. Archives of Civil and Mechanical Engineering, 18 (2018), No 4, 1729-1742.

[3] Fiala P., Drexler P., Nešpor D., Szabó Z., Mikulka J., Polívka J., The Evaluation of Noise Spectroscopy Tests, ENTROPY, 18 (2016), No. 12, 1-16.

[4] Krawczyk A., Korzeniewska E., Łada-Tondyra, E. Magnetophosphenes – History and contemporary implications, Przeglad Elektrotechniczny, 94 (2018), No 1, 61-64.

[5] Korzeniewska E., Walczak M., Rymaszewski J., Elements of Elastic Electronics Created on Textile Substrate, Proceedings of the 24th International Conference Mixed Design of Integrated Circuits and Systems - MIXDES 2017, 2017, 447-45.

[6] Lopato P., Chady T., Sikora R., Ziolkowski M., Full wave numerical modelling of terahertz systems for nondestructive evaluation of dielectric structures, 32 (2013), No. 3, 736 – 749.

[7] Psuj G., Multi-Sensor Data Integration Using Deep Learning for Characterization of Defects in Steel Elements, Sensors, 18 (2018), No. 1, 292.

[8] Szczęsny A., Korzeniewska E., Selection of the method for the earthing resistance measurement, Przegląd Elektrotechniczny, 94 (2018), No. 12, 178-181.

[9] Valis D., Mazurkiewicz D., Application of selected Levy processes for degradation modelling of long range mine belt using real-time data, Archives of Civil and Mechanical Engineering, 18 (2018), No. 4, 1430-1440.

[10] Valis D., Mazurkiewicz D., Forbelska M., Modelling of a Transport Belt Degradation Using State Space Model, Conference: IEEE International Conference on Industrial Engineering and Engineering Management (IEEE IEEM)Location: Singapore, Dec. 10-13, 2017, Book Series: International Conference on Industrial Engineering and Engineering Management IEEM, 2017, 949-953.

[11] Ziolkowski M., Gratkowski S., and Zywica A. R., Analytical and numerical models of the magnetoacoustic tomography with magnetic induction, COMPEL - Int. J. Comput. Math. Electr. Electron. Eng., 37 (2018), No. 2, 538–548.

[12] Kozłowski E., Mazurkiewicz D., Żabiński T., Prucnal S., Sęp J., Assessment model of cutting tool condition for real-time supervision system, Eksploatacja i Niezawodnosc – Maintenance and Reliability, 21 (2019); No 4, 679–685.

[13] Vališ D, Hasilová K., Forbelská M, Vintr Z, Reliability modelling and analysis of water distribution network based on backpropagation recursive processes with real field data, Measurement 149 (2020), 107026.

[14] Galazka-Czarnecka, I.; Korzeniewska E., Czarnecki A. et al., Evaluation of Quality of Eggs from Hens Kept in Caged and Free-Range Systems Using Traditional Methods and Ultra-Weak Luminescence, Applied sciences-basel, 9 (2019), No. 12, 2430.

[15] Babout L., Grudzień K., Wiącek J., Niedostatkiewicz M., Karpiński B., and Szkodo M., Selection of material for X-ray tomography analysis and DEM simulations: comparison between granular materials of biological and non-biological origins, Granul. Matter, 20 (2018), No. 3, 38.

[16] Chaniecki Z., Romanowski A., Nowakowski J., Niedostatkiewicz M., Application of twin-plane ECT sensor for identification of the internal imperfections inside concrete beams Grudzien, IEEE Instrumentation and Measurement Technology Conference, 2016, 7520512.

[17] Herman G.T., Image Reconstruction from Projections: The Fundamentals of Computerized Tomography, Academic Press, New York, 1980.

[18] Holder D., Introduction to biomedical electrical impedance tomography Electrical Impedance Tomography Methods, History and Applications, Bristol, Institute of Physics, 2005.

[19] Karhunen K., Seppänen A., Lehikoinen A., Monteiro P. J., and Kaipio J. P., Electrical Resistance Tomography Imaging of Concrete, Cement and Concrete Research, 40 (2010), 137–145.

[20] Gudra T., Opieliński K.J., The multi–element probes for ultrasound transmission tomography, Journal de Physique 4, 137 (2006), 79–86.

[21] Jiang Y., Soleimani M., Wang B., Contactless electrical impedance and ultrasonic tomography, correlation, comparison and complementary study, Measurement Science and Technology, 30 (2019), 114001.

[22] Kaczmarz S., Angenäherte Auflösung von Systemen Linearer Gleichungen, Bull. Acad. Polon. Sci. Lett. A, 6–8A (1937), 355–357.

[23] Kak A.C., Slaney M., Principles of Computerized Tomographic Imaging, IEEE Press, New York, 1999.

[24] Nityananda R., Samuel J., Fermat's principle in general relativity, Physical review D: Particles and fields, June 1992.

[25] Polakowski K., Sikora J., Podstawy matematyczne obrazowania ultradźwiękowego, Politechnika Lubelska, Lublin, 2016.

[26] Kryszyn J., Wanta D. M., Smolik W. T., Gain Adjustment for Signal-to-Noise Ratio Improvement in Electrical Capacitance Tomography System EVT4, IEEE Sens. J., 17 (2017), No. 24, 8107–8116.

[27] Kryszyn J., Smolik W., Toolbox for 3d modelling and image reconstruction in electrical capacitance tomography, Informatyka, Automatyka, Pomiary w Gospodarce i Ochronie Środowiska (IAPGOŚ) , 7 (2017), No. 1, 137-145.

[28] Majchrowicz M., Kapusta P., Jackowska-Strumiłło L., Sankowski D., Optimization of Distributed Multi-node, Multi-GPU, Heterogeneous System for 3D Image Reconstruction in Electrical Capacitance Tomography, Image processing & communications, 21 (2016), No. 3, 2016, 81-90.

[29] Nowakowski J., Ostalczyk P., Sankowski D., Application of fractional calculus for modelling of two-phase gas/liquid flow system, Informatyka, Automatyka, Pomiary w Gospodarce i Ochronie Środowiska (IAPGOŚ) , 7 (2017), No. 1, 42-45.

[30] Romanowski A., Contextual Processing of Electrical Capacitance Tomography Measurement Data for Temporal Modeling of Pneumatic Conveying Process, 2018 Federated Conference on Computer Science and Information Systems (FedCSIS), IEEE, 2018, 283-286.

[31] Rymarczyk T, Kłosowski G. Innovative methods of neural reconstruction for tomographic images in maintenance of tank industrial reactors. Eksploatacja i Niezawodnosc – Maintenance and Reliability, 21 (2019); No. 2, 261–267

[32] Rymarczyk, T.; Kozłowski, E.; Kłosowski, G.; Niderla, K. Logistic Regression for Machine Learning in Process Tomography, Sensors, 19 (2019), 3400.

[33] Rymarczyk T., Szumowski K., Adamkiewicz P., Tchórzewski P., Sikora J., Moisture Wall Inspection Using Electrical Tomography Measurements, Przegląd Elektrotechniczny, 94 (2018), No 94, 97-100

[34] Duda K., Adamkiewicz P., Rymarczyk T., Niderla K., Nondestructive Method to Examine Brick Wall Dampness, International Interdisciplinary PhD Workshop Location: Brno, Czech Republic Date: SEP 12-15, 2016, 68-71

[35] Rymarczyk T., Nita P., Vejar A., Stefaniak B., Sikora J., Electrical tomography system for Innovative Imaging and Signal Analysis, Przegląd Elektrotechniczny, 95 (2019), No 6, 133-136

[36] Soleimani M., Mitchell CN, Banasiak R., Wajman R., Adler A., Four-dimensional electrical capacitance tomography imaging using experimental data, Progress In Electromagnetics Research, 90 (2009), 171-186.

[37] Wajman R., Fiderek P., Fidos H., Sankowski D., Banasiak R., Metrological evaluation of a 3D electrical capacitance tomography measurement system for two-phase flow fraction determination, Measurement Science and Technology, 24 (2013), No. 6, 065302.

[38] Wang M., Industrial Tomography: Systems and Applications, Elsevier, 2015.

[39] Ye Z., Banasiak R., Soleimani M., Planar array 3D electrical capacitance tomography, Insight: Non-Destructive Testing and Condition Monitoring, 55 (2013), No. 12, 675-680

[40] Romanowski, A.; Łuczak, P.; Grudzień, K. X-ray Imaging Analysis of Silo Flow Parameters Based on Trace Particles Using Targeted Crowdsourcing, Sensors, 19 (2019), No. 15, 3317.